Astronomy & Astrophysics manuscript no. master
September 30, 2016

SWEET-Cat update and FASMA

A new minimization procedure for high quality spectra⋆

D. T. Andreasen[1,2], S. G. Sousa[1], M. Tsantaki[3], G. Teixeira[1], A. Mortier[4], N. C. Santos[1,2], L. Suárez-Andrés[5,6], and E. Delgado-Mena[1]

[1] Instituto de Astrofísica e Ciências do Espaço, Universidade do Porto, CAUP, Rua das Estrelas, 4150-762 Porto, Portugal e-mail: daniel.andreasen@astro.up.pt
[2] Departamento de Física e Astronomia, Faculdade de Ciências, Universidade do Porto, Rua Campo Alegre, 4169-007 Porto, Portugal
[3] Instituto de Radioastronomía y Astrofísica, IRyA, UNAM, Campus Morelia, A.P. 3-72, 58089 Michoacán, Mexico
[4] SUPA, School of Physics and Astronomy, University of St Andrews, St Andrews KY16 9SS, UK
[5] Depto. Astrofísica, Universidad de La Laguna (ULL), E-38206 La Laguna, Tenerife, Spain
[6] Instituto de Astrofísica de Canarias, E-38205 La Laguna, Tenerife, Spain

Received ...; accepted ...

ABSTRACT

Aims.
Methods.
Results.

Key words. data reduction: high resolution spectra – stars individual: Arcturus – stars individual: HD010853

1. Introduction

The study of extrasolar planetary systems is an established field of research. To date, nearly 3500 extrasolar planets have been discovered around almost 2500 solar-type stars[1]. Most of these have been found thanks to the incredible precision achieved in photometric transit and radial velocity methods. Not only do we have intriguing new types of planetary systems that challenge current theories but also the increasing number of exoplanets allows us to do statistical studies of the newfound worlds by analyzing their internal structure, atmospheric composition, and planetary composition.

Precise and accurate planetary parameters (mass, radius, and mean density) are needed to distinguish between solid rocky, water rich, gaseous, or otherwise composed planets. A key aspect to this progress is the characterization of the planet host stars. For instance, precise and accurate stellar radii are critical if we want to measure precise and accurate values of the radius of a transiting planet (see e.g. Torres et al. 2012; Mortier et al. 2013). The determination of the stellar radius is in turn dependent on the quality of the derived stellar atmospheric parameters such as the effective temperature.

We continue the work of Santos et al. (2013) by deriving atmospheric parameters, namely the effective temperature ($T_{\rm eff}$), surface gravity ($\log g$), metallicity ([Fe/H], where iron often is used as a proxy for the total metallicity), and the micro turbulence ($\xi_{\rm micro}$) in a homogeneous way for a sample of planet host stars. This, in turn, allows us to study new correlations between planets and their hosts in a homogeneous way, or gain higher statistical certainty on the already discovered correlations.

The analysis of high quality spectra, i.e. spectra with high spectral resolution and a high signal to noise ratio (SNR), serves an important role in the derivation of stellar atmospheric parameters. Nevertheless, spectral analysis is a time consuming method. There has been an increase of the amount of optical high-resolution spectrographs available and, additionally, a number of near-IR spectrographs are either planned or are already available making the task of analyzing the increasing amount of spectra even more crucial.

In the era of large data sets, computation time has to be decreased as much as possible without compromising the quality of the results. In the light of this we have developed a tool to derive atmospheric parameters in a fast and robust way using standard spectroscopic methods. We made this tool available as a web interface at `linktoFASMA`. This works well for optical spectra which we demonstrate in Section 3.4 using the line list from Sousa et al. (2011). This tool also ships with a line list for near-IR spectra using the line list presented recently in Andreasen et al. (2016). The tool is provided to the community as an easy to use web tool to avoid any problems with installations. The tool is described in detail in Section 3.

2. Data

In this paper we derived parameters for a sample of 66 stars, 43 were observed by our team using the UVES (Dekker et al. 2000), FEROS (Kaufer et al. 1999), and FIES (Frandsen & Lindberg 1999) spectrographs. The rest (23) spectra were found in various archives. Additionally, we use spectra from HARPS (Mayor et al. 2003) and ESPaDOnS (Donati 2003). Some characteristics of the spectrographs are presented in Table 1 with the mean SNR for the spectra used. The SNR for each star can be seen in Table .1 along with the atmospheric parameters of the stars.

⋆ Data is from the following program IDs: 092.C-0695, 093.C-0219,2014B/020, 094.C-0367, 095.C-0324, and 096.C-0092.

[1] For an updated table we refer to http://www.exoplanet.eu

We obtain the spectra with the highest possible resolution for a given spectrograph, and in cases with multiple observations, we include all unless a spectrum is close to the saturation limit for a given spectrograph. For multiple spectra, we combine them after first correcting the radial velocity (RV) and using a sigma clipper to remove cosmic rays. The individual spectra are then combined to a single spectrum for a given star to increase the SNR. This single spectrum is used in the analysis below. For most of the spectra in the archive included here, several spectra were combined as described above, while for the observations dedicated to this work, the spectrum would be a single spectrum. This is mostly due to the difference in science cases behind the observations. E.g. the HARPS spectra were used for RV monitoring or follow up of the exoplanet(s), while the UVES spectra were used for characterisation of stellar parameters.

Table 1. Spectrographs used for this paper with their spectral resolution, wavelength coverage, and typical (mean) SNR from the spectra used.

Spectrograph	Resolution	Spectral coverage	Mean SNR
UVES	110 000	480 – 680 nm	212
FEROS	48 000	350 – 920 nm	208
HARPS	115 000	378 – 691 nm	642
FIES	67 000	370 – 730 nm	763
ESPaDOnS	81 000	370 – 1050 nm	775

3. FASMA

FASMA (acronym for Fast Analysis of Spectra Made Automatically) is a web tool[2] for analyzing spectra. FASMA is written in Python and works as a wrapper around ARES (Sousa et al. 2015) and MOOG (Sneden 1973, version 2014), for an all-in-one tool. ARES is a tool to automatically measure equivalent widths (EW) from a spectrum given a line list. MOOG is a radiative transfer code under the assumption of local thermodynamic equilibrium (LTE).

FASMA has three different modes: i) Measure EWs using ARES, ii) derive stellar parameters from a set of measured Fe I and Fe II line EWs, and iii) abundances derivation for 15 elements, all described below. The model atmospheres are formatted in a grid of Kurucz Atlas 9 plane-parallel, 1D static model atmospheres Kurucz (1993). FASMA can also manage the new grid of Atlas models calculated by Mészáros et al. (2012) for the APOGEE survey and the MARCS models (Gustafsson et al. 2008). The interpolation from the grid is calculated from a geometric mean for effective temperature, surface gravity and metallicity.

3.1. EW measurements

The EWs are strongly correlated with the atmospheric parameters. Measurements of the EW can be done manually using a tool like splot in IRAF, but often when dealing with a large sample of stars this is not a suitable way to deal with the task. Therefore tools like ARES exist which can measure the EWs of spectral lines automatically. To use this mode of FASMA, it just needs a spectrum (format should be 1D fits for ARES to read it) and a line list[3]. For the latter, FASMA is shipped with some line lists ready to use, in the format suitable for FASMA. The output will be a line list in the format required for MOOG. The output can be used for either the EW method or the abundance method, both described below.

The line lists shipped with FASMA are presented in Table 2. These line lists are all calibrated for the Sun, i.e. the oscillator strengths for each absorption line are changed so the line with the measured EW from a solar spectrum return solar abundance for the given element.

Table 2. The line lists provided with FASMA. The first two line lists are for parameter determination while the last line list is used to derive abundances for 15 different elements.

Line list	Fe I/Fe II	Elements	Usage
Sousa et al. (2008)	263/36	1	Parameters
Tsantaki et al. (2013)	120/17	1	Parameters
Andreasen et al. (2016)	249/5	1	Parameters
Neves et al. (2009)	-/-	15	Abundances

3.2. Stellar parameter derivation

The standard determination of spectroscopic parameters for solar-type stars starts by measuring the EW of selected and well-defined absorption lines. Then we translate these measurements into individual line abundances, assuming a given atmospheric model. We obtain the correct stellar parameters by imposing excitation and ionization balance for the iron species.

- The effective temperature has a strong influence on the correlation of iron abundance with the excitation potential (excitation balance). We obtain the $T_{\rm eff}$ when Fe I abundance shows no dependence on the excitation potential, i.e., the slope of abundance versus excitation potential is zero.
- Surface gravity is derived from the ionization balance of Fe I and Fe II abundances. Therefore, the abundance of neutral iron should be equal to the abundance of ionized and consistent with the one of the input model atmosphere.
- Microturbulence is connected with the saturation of the stronger iron lines. However, the abundances for weak and strong lines of a certain species (in our case iron) should be the same independent of the value of $\xi_{\rm micro}$. Iron abundances should show no dependence on the reduced equivalent width, i.e. the slope of abundance vs the reduced EW is zero.

With measured EWs of Fe I and Fe II lines we calculate abundances using a stellar atmosphere model for a given set of atmospheric parameters ($T_{\rm eff}$, $\log g$, [Fe/H], and $\xi_{\rm micro}$). By removing correlations between the measured abundances (through the measured EWs) and the excitation potential (EP) and reduced EW ($\log(EW/\lambda)$) we can constrain $T_{\rm eff}$ and $\xi_{\rm micro}$. By obtaining ionization balance between Fe I and Fe II (that is the average abundance of all Fe I lines are equal to the average abundance of all Fe II lines) we constrain $\log g$. Lastly, we change the input [Fe/H] to match that of the average output [Fe/H]. Hence we have four criteria to minimize simultaneously:

1. The slope between abundance and excitation potential ($a_{\rm EP} \leq 0.001$).
2. The slope between abundance and reduced EW ($a_{\rm RW} \leq 0.003$). We use 0.003 rather than 0.001 since this slope varies more rapidly with small changes in atmospheric parameters.
3. The difference between the average abundances of Fe I and Fe II (ΔFe ≤ 0.01).

[2] super-cool-address-with-FASMA
[3] ARES does in principle just need a list of wavelengths in order to run, but is often used with a line list with characteristics of the atomic absorption line.

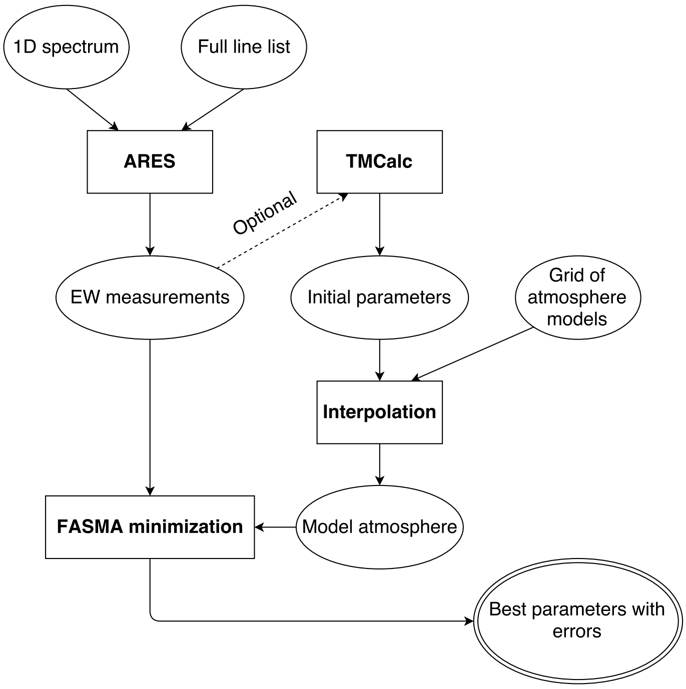

Fig. 1. A general overview over FASMA from spectrum to parameters.

4. Input and output metallicity should be equal.

These criteria we denote as indicators for the physical parameters which we are trying to minimize for. We denote this method for obtaining stellar parameters for the EW method.

There exists many minimization routines available in Python. Most commonly known are the ones from the SciPy ecosystem[4]. There are some pros and cons with using proprietary minimization routines. Pros are that it is already written, and usually there is good documentation for libraries such as SciPy. Cons in this situation is, that most minimization routines do not work well with vector functions returning another vector:

$$f(\{T_{\rm eff}, \log g, [Fe/H], \xi_{\rm micro}\}) = \{a_{\rm EP}, a_{\rm RW}, \Delta{\rm Fe}\ , {\rm Fe\,I}\}. \quad (1)$$

A work around is to combine the criteria into one single criteria by e.g. adding them quadratically and minimize that expression instead. Thus we have a vector function returning a scalar:

$$f(\{T_{\rm eff}, \log g, [Fe/H], \xi_{\rm micro}\}) = \sqrt{a_{\rm EP}^2 + a_{\rm RW}^2 + \Delta{\rm Fe}\ ^2}. \quad (2)$$

The minimization routines are also not physical in the sense that they are not optimized for the problem. These two cons were incitement for writing a minimization routine optimized for the problem at hand. Here is how it works.

1. Run MOOG once with user defined initial parameters (default is solar) and calculate $a_{\rm EP}$, $a_{\rm RW}$, and ΔFe .
2. Change the atmospheric parameters ($T_{\rm eff}$, $\log g$, [Fe/H], $\xi_{\rm micro}$) according to the size of the indicator. A parameter is only changed if it is not fixed.
   – $a_{\rm EP}$: Indicator for $T_{\rm eff}$. If this value is positive, then increase $T_{\rm eff}$.
   – $a_{\rm RW}$: Same as above but for $\xi_{\rm micro}$.
   – ΔFe : Positive ΔFe means $\log g$ should be decreased and vice versa.

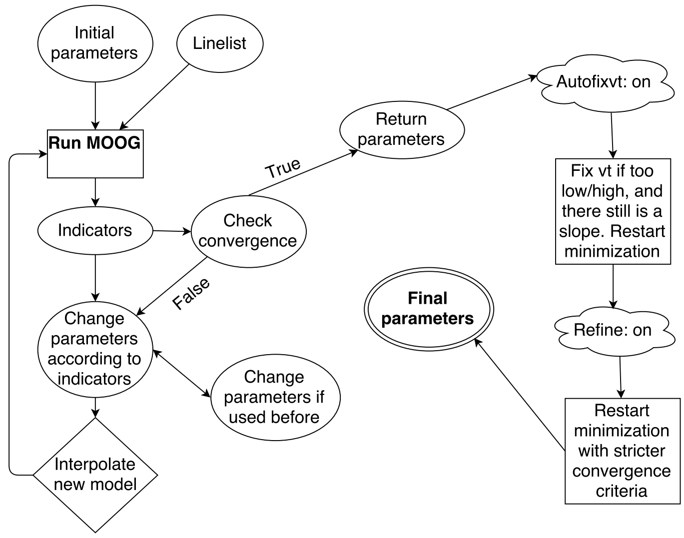

Fig. 2. A schematic overview over the minimization for FASMA with the EW method.

   Fe / is changed to the output [Fe/H] in each iteration.
3. If the new parameters have already been used in a previous iteration, then change them slightly. This is done by drawing a random number from a Gaussian distribution with a mean at the current value and a sigma equal to the absolute value of the indicator.
4. Calculate a new atmospheric model by interpolating a grid of models so we have the requested parameters and run MOOG once again.
5. For each iteration save the parameters used and the quadratic sum of the indicators. If we do not reach convergence, then return the best found parameters.

This whole process is schematically shown in Figure 1 and the minimization routine itself in Figure 2. The stepping follows these simple equations:

$$T_{\rm eff} \mathrel{+}= 2000\,{\rm K} a_{\rm EP} \quad (3)$$

$$\xi_{\rm micro} \mathrel{+}= 1.5\,{\rm km/s} a_{\rm RW} \quad (4)$$

$$\log g \mathrel{-}= \Delta{\rm Fe}\,. \quad (5)$$

The metallicity is corrected at each step so the input metallicity matches that of the output metallicity of the previous iteration. The functional form for changing the parameters were found by changing one parameter, e.g. $T_{\rm eff}$, while keeping the other parameters fixed at their convergence values. A linear fit was applied to $T_{\rm eff} - T_{\rm eff,0}$ vs. $a_{\rm EP}$ in order to get the slope. Since we ignore all interdependencies between the parameters in doing so, we lower the slopes above a little and arrive to these very simple equations.

The error estimates are based on the same method presented in Gonzalez & Laws (2000), which is also described in detail in Santos et al. (2003); Andreasen et al. (2016).

By using the indicators like this, we can relatively fast reach convergence. Typical calculation time for an FGK dwarf with a high quality spectrum is around 2 min.

3.2.1. Options

It is possible to run the EW method with a set of different options which will be described here.

[4] `http://scipy.org`

- *fixteff*: Fix $T_{\rm eff}$ and derive the other parameters. Same is available for $\log g$ (*fixlogg*), [Fe/H] (*fixfeh*), and $\xi_{\rm micro}$ (*fixvt*). One or more parameters can be fixed. When one or more parameters are fixed, the corresponding indicator will be ignored for each iteration, thus the parameter itself will not be changed.
- *outlier*: Remove a spectral line(s) after the the minimization is done, if the abundance of this spectral line is more than 3σ away from the average abundance of all the lines. After the removal of outlier(s) the minimization routine restarts. The options are to remove all outliers above 3σ once or iteratively, or remove one outlier above 3σ once or iteratively.
- *autofixvt*: If the minimization routine does not converge and $\xi_{\rm micro}$ is close to 0 or 10 with a significant $a_{\rm RW}$ (numerically bigger than 0.05), then fix $\xi_{\rm micro}$. This option was added since we saw this behaviour in some cases. The solution was typically to restart the minimization manually with $\xi_{\rm micro}$ fixed. If $\xi_{\rm micro}$ is fixed it is changed at each iteration according to an empirical relation. For dwarfs it follows the one presented in Tsantaki et al. (2013) and for giants it follows the one presented in Adibekyan et al. (2015).
- *refine*: After the minimization is done, run it again from the best found parameters but with more strict criteria. If this option is set, it will always be the last step (after removal of outliers). The convergence criteria can be changed by the user, but we recommend using the defaults provided above.
- *tmcalc*: Use TMCalc (Sousa et al. 2012) to fast estimate the $T_{\rm eff}$ and [Fe/H] using the raw output from ARES. We then assume solar surface gravity (4.44 dex) and estimate $\xi_{\rm micro}$ based on an empirical relation (see below).

We use the line list presented in Sousa et al. (2008). However, this line list does not work well for cool stars. This was fixed in Tsantaki et al. (2013) by removing some lines from Sousa et al. (2008). For stars cooler than 5200 K we automatically rederive the atmospheric parameters after removing lines so the line list resemble that of Tsantaki et al. (2013). The line list for the NIR is also available (Andreasen et al. 2016).

All restarts of the minimization routine is done with initial condition at the last found best parameters.

3.3. Abundance method

FASMA calculates element abundances for 12 elements (Na, Mg, Al, Si, Ca, Ti, Cr, Ni, Co, Sc, Mn, and V) from spectral lines determined in Neves et al. (2009) and Adibekyan et al. (2012). The atomic data were calibrated with the Sun as reference and solar abundances from Anders & Grevesse (1989). The EWs are measured automatically with the ARES mode of FASMA. The element abundance of each line is derived using the atmospheric parameters of the stars obtained from the previous step. The final element abundance of each star is calculated from the average value of the abundances produced by all lines detected in a given star and element.

3.4. Testing FASMA

To test the EW method implemented in FASMA we derive parameters from the 582 sample by Sousa et al. (2011). This sample has a wider range of SNR than the 451 sample from Tsantaki et al. (2013), therefore making it better for a comparison. We use ARES2 to measure the EWs. ARES can give an estimate on the signal to noise ratio (SNR) by analyzing the continuum in given intervals. For solar type stars the following intervals are working well: 5764-5766 Å, 6047-6053 Å, and 6068-6076 Å. From the estimated SNR, ARES can give an estimate on the very important *rejt* parameters (see Sousa et al. 2015, for more information). After measuring the EWs with ARES, we use the FASMA minimization described in Section 3.2 to determine the stellar atmospheric parameters. The results are presented in Figure 3 which shows $T_{\rm eff}$, $\log g$, [Fe/H], and $\xi_{\rm micro}$ for FASMA against those of Sousa et al. (2011).

The sample contains stars with $T_{\rm eff}$ too cold for the line list used. As described in Section 3.2 we should then convert the line list by Sousa et al. (2008) to the line list presented in Tsantaki et al. (2013). However, since this line list was not available when Sousa et al. (2011) derived parameters, we do not make this change in order to make a fair comparison for FASMA.

The mean of the difference between parameters from Sousa et al. (2011) and those by FASMA are presented in Table 3.

Table 3. The difference in derived parameters by Sousa et al. (2011) and FASMA. Second column is the mean difference with EWs measured by ARES in FASMA, while the third column is the mean difference using 20 randomly stars with the exact same EWs.

Parameter	Mean difference	Same line list
$T_{\rm eff}$	16 ± 36 K	21 ± 11 K
$\log g$	-0.04 ± 0.07	-0.007 ± 0.009
[Fe/H]	0.03 ± 0.02	0.004 ± 0.009
$\xi_{\rm micro}$	-0.04 ± 0.14 km/s	0.04 ± 0.02 km/s

The comparison is very consistent as expected and the small offsets are within the errors except for metallicity. This can be due to different versions of MOOG, measured line lists, interpolation of atmosphere grid, and minimization routine. Most likely the difference will be due to different used *rejt* parameters in ARES, which can alter the EWs systematically and hence the metallicity. We therefore randomly selected 20 stars with different $T_{\rm eff}$ and used the EWs directly from Sousa et al. (2011) to derive parameters. The results are presented in the last column of Table 3. We note that the $\log gf$ values from the original line lists by Sousa et al. (2011), which used the MOOG 2002 version, were not changed for the 2014 version of MOOG. This might lead to some errors as well. However, the offsets are very small and compatible with the errors on parameters normally obtained from high quality spectra.

3.5. Web interface

NOTE: More will be written once we have a web page.

We provide a web interface for FASMA. In the web interface it is possible to use some of the line list provided with FASMA to measure EWs of a spectrum (has to be provided by the user). This can be used for all the available FASMA methods described above.

The web interface can be found at the following link `super-cool-address-with-FASMA`.

4. New homogeneous spectroscopic parameters for 66 planet hosts

Here we present the sample of 66 stars. We were unable to derive parameters for HD77065. This is a spectroscopic binary according to Pourbaix et al. (2004), and the spectrum is contaminated with the companion star. This make EW measurement very difficult, hence we exclude it from the sample of collected spectra.

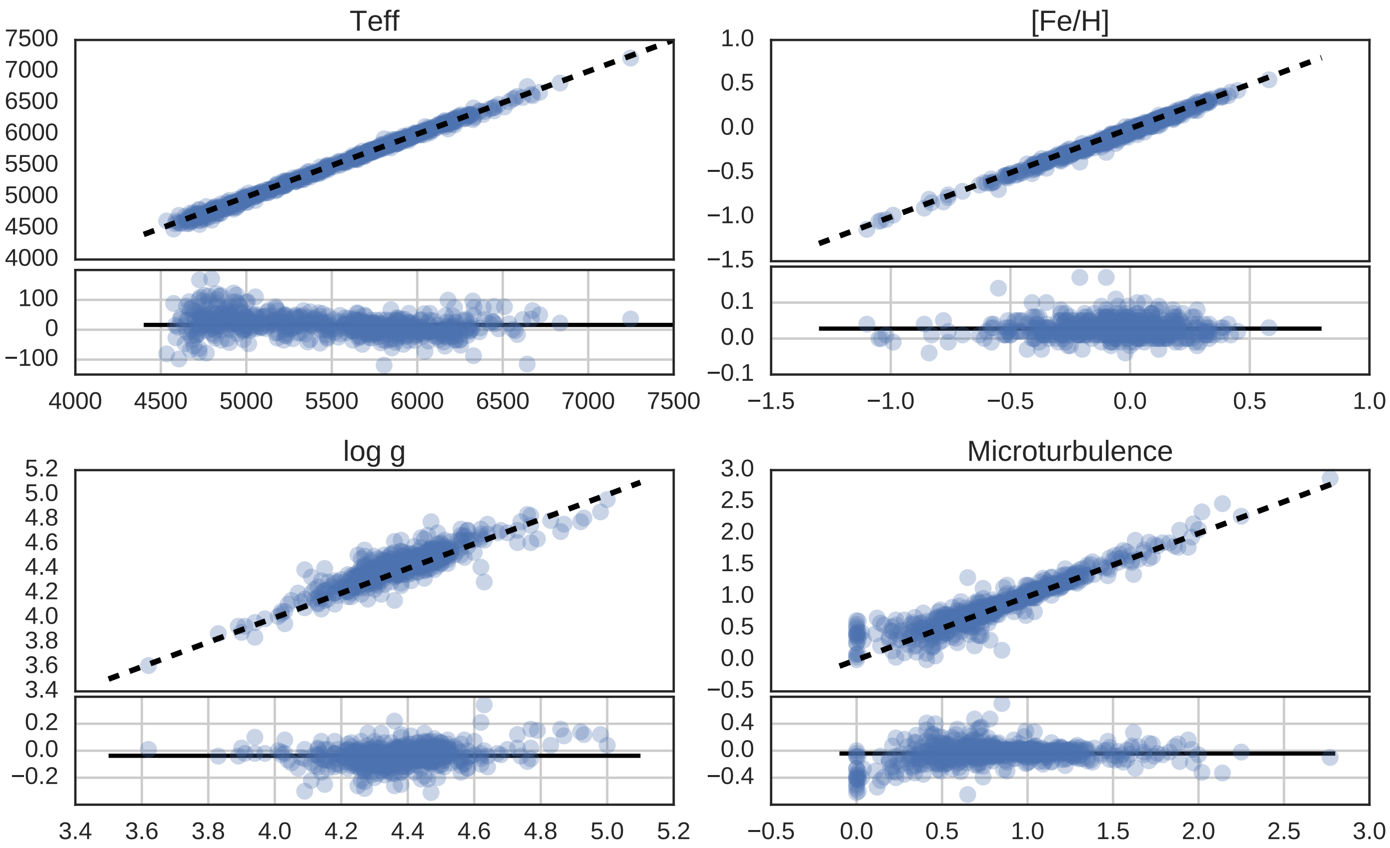

Fig. 3. Stellar atmospheric parameters derived by FASMA compared to the sample by Sousa et al. (2011). The x-axis in all plots show the results from FASMA while the y-axis is the parameters derived by Sousa et al. (2011).

Moreover we were not able to successfully derive parameters with this method for Aldebaran, a well known red giant star. Even though the quality of the spectra for a bright star like Aldebaran are available, the spectral type is intrinsic difficult due to the low $T_{\rm eff}$ which can give arise to molecular absorption in the optical. We also expect to see non-LTE effects for this kind of spectral type. That we are not able to derive parameters for Aldebaran is not a big concern, since it is well studied with other techniques, and we can trust the parameters already listed in SWEET-Cat.

Last, we also removed 19 from our sample since these stars did not convergence during the minimization procedure. The $T_{\rm eff}$ for these stars is either too hot or too cold for the EW method to work.

The remaining 66 stars are presented in Table .1. Note that we apply a correction to the spectroscopic $\log g$ based on asteroseismology as found in Mortier et al. (2014). We only use this corrections for FGK dwarf stars, i.e. between 4800 K $\leq T_{\rm eff} \leq$ 6500 K and $\log g \geq 4.2$. For stars with a $\log g$ lower than this limit we do not apply the corrections, and if the $\log g$ change to below this limit after the correction, we go back to use the spectroscopic $\log g$ again.

We present a Hertzprung-Russel diagram (HRD) of our sample in Figure 4. Figure 4 is made with a tool for post processing the results saved to a table by FASMA.

We present the new atmospheric parameters in Figure 5 against the literature values which were in SWEET-Cat before

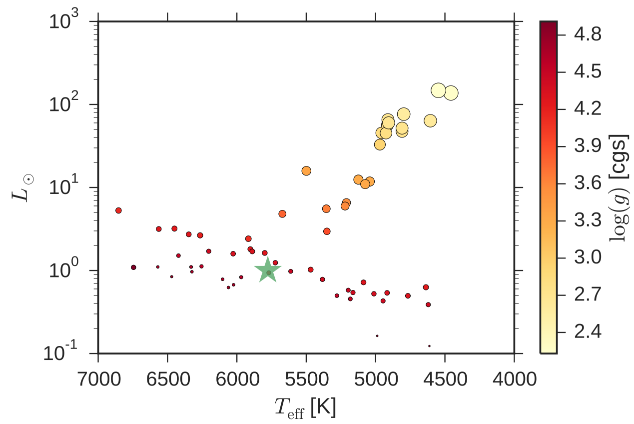

Fig. 4. Hertzprung-Russel diagram of our sample with the Sun as a green star. The size of the points represents the $\log g$, with bigger points being smaller $\log g$ (giants), and vice versa. The colour code show the same as the size. Red points are the dwarfs, while yellow points are the giants.

this update. With 2461 stars discovered with planets, 21% of these stars have been analyzed in the homogeneous way as described in this work. We note that the limiting factor at the moment for increasing the sample of stars analyzed in the homo-

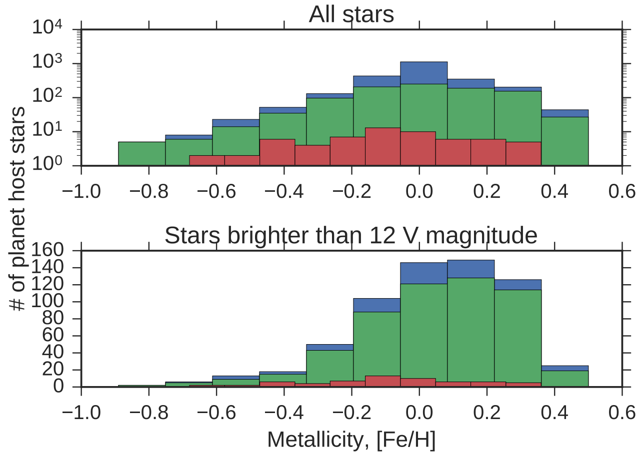

Fig. 6. The metallicity distribution. In the *upper* plot we see all stars (logarithmic scale) in SWEET-Cat, divided in three. Blue (the largest distribution) are all stars available in SWEET-Cat, green (the middle distribution) are the stars with homogenity flag 1, i.e. analyzed using the method described in this paper, red (the smallest distribution) are all new stars added from this paper. The *lower* plot show a 12 V magnitude cut to exclude stars which are currently unavailable spectroscopically.

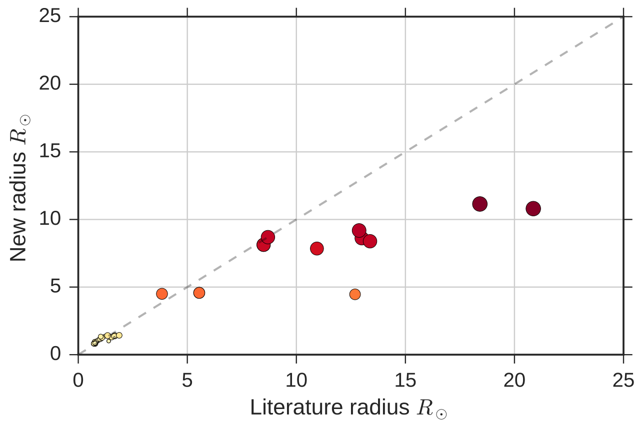

Fig. 7. The stellar radius on both axis calculated based on Torres et al. (2010). For the x-axis we show the stellar radius based on the atmospheric parameters from the literature, while the y-axis is from the new homogeneous parameters presented here. The colour and size present the surface gravity. This clearly shows that the disagreement is biggest for more evolved stars.

geneous way is the magnitude of that planet hosts. There have been found many planet hosts with space mission as *Kepler* and *CoRoT* using the transiting method. Most of these stars are faint and thus making them time expensive for the spectroscopic analysis required here. For stars brighter than magnitude 12 the completeness, i.e. the stars analyzed in a homogeneous way compared to the ones we did not analyze yet, is up to 77% now while it is at 85% for exoplanet hosts brighter than magnitude 10.

The metallicity distribution for all the planet host stars are important to understand e.g. planet formation. We present a distribution in Figure 6. The sample is divided in two, for all stars, and for stars brighter than 12 V magnitude. Stars dimmer are mainly observed with the *Kepler* space mission. These dim stars are very time consuming, and hence expensive to observe.

5. Discussion

We will now focus on the stars with $T_{\rm eff}$ higher than 4800 K and lower than 6500 K. Outside this range the EW method suffers from different factors and will be less reliable. For the lower range, we expect to see more line blending, and hence the EW measurements will no longer be reliable. Without reliable EW measurements, the rest of the technique will not work. For the other limit we start to see non-LTE effects which we do not take into account, hence the method does not work there (Gray 2005).

We compute radius and mass of all stars (even the ones which parameters may not be reliable in order to be complete) using the empirical formula presented in Torres et al. (2010). Some of the stars have derived radius from different methods and generally show a good correlation with radius derived from Torres et al. (2010) if the literature parameters of $T_{\rm eff}$, $\log g$, and [Fe/H] are used. However, if we compare with the new radius derived using the parameters presented here the results can differ up to 65%. We show in Figure 7 how the radius calculated from Torres et al. (2010) differ between the literature atmospheric parameters and the new homogeneous atmospheric parameters presented here. We note that stellar radii is provided by many of the authors from different discovery papers, but we chose to compare the atmospheric parameters via the derivation of the stellar radius as described above, rather than compare the stellar radii from different methods.

Below we discuss the systems where the radius of the stars changes more then 25% and how this influences the planetary parameters. The changes in radius for a star is primarily due to changes in $\log g$, which can be used as an indicator of the evolutionary stage of a star.

The 7 stars (8 exoplanets) which radius deviates more than 25% are discussed below. We rederive the planetary radius, mass and semi-major axis when possible following the three simple relations:

$$M_{\rm pl,new} = \left(\frac{M_{*,\rm lit}}{M_{\rm st,new}}\right)^{-2/3} M_{\rm pl,lit} \quad (6)$$

$$R_{\rm pl,new} = \left(\frac{R_{*,\rm lit}}{R_{\rm st,new}}\right) R_{\rm pl,lit} \quad (7)$$

$$a_{\rm pl,new} = \left(\frac{M_{*,\rm lit}}{M_{\rm st,new}}\right)^{1/3} a_{\rm pl,lit}, \quad (8)$$

where subscript lit denotes the value from the literature which we compare with, subscript new will be the new computed values, subscript pl is short for planet, and last subscript $*$ is short for star. M, R, and a are mass, radius, and semi-major axis respectively. Note that for the literature values, we use the values reported directly from the literature, and not the derived radius and mass from Torres et al. (2010). To identify outliers, we compare radii and masses derived from Torres et al. (2010) since this is a measure of how the atmospheric parameters have changed.

5.1. HAT-P-46

HAT-P-46 has two discovered exoplanets according to Hartman et al. (2014). The outer planet HAT-P-46 c is not transiting hence we do not have any radius for this planet. The results we present in this paper for this star comes from UVES data with a SNR at 208. Hartman et al. (2014) derives the following spectroscopic parameters: $T_{\rm eff} = 6120 \pm 100$ K, $\log g = 4.25 \pm 0.11$, and [Fe/H] = 0.30 ± 0.10. We note that for this star the asteroseismic correction we apply as mentioned in Section 4, the corrected

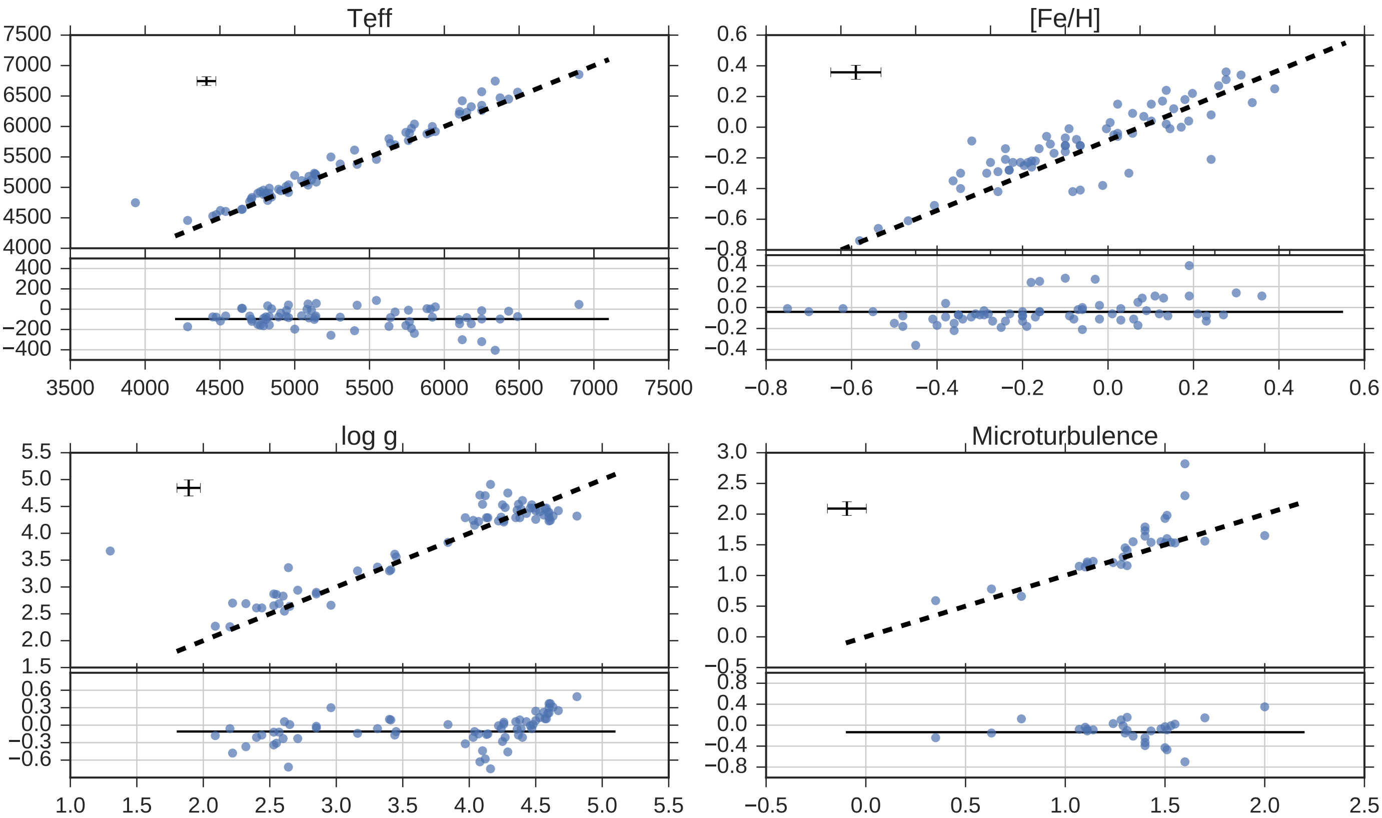

Fig. 5. Atmospheric parameters of the updated planet host stars. The x-axis are the previous values in SWEET-Cat (usually from the discovery paper of the exoplanet), while the y-axis is the new updated values. In the upper left corner of each of the four plots we show the typical error on the parameters.

$\log g$ were below 4.2dex, so we end up using the spectroscopic $\log g$ for this star.

If we derive the mass and radius of HAT-P-46 b with our new parameters, we obtain the following: $R_{\rm pl} = 0.93 R_J$, while Hartman et al. (2014) derived $R_{\rm pl} = 1.28 R_J$ in units of Jupiter. We see no change in mass (Hartman et al. (2014) found $M_{\rm pl} = 0.49 R_J$), however there is a decrease in the radius, and we end up with a more dense planet, $\rho_{\rm pl} = 0.76$ from $\rho_{\rm pl} = 0.28 \pm 0.10$.

As the secondary companion does not transit we only have a limit on the minimum mass for this planet. Here we get: $M \sin i_{\rm pl} = 1.97(2.00) R_J$, so a very small change as expected.

5.2. HD 120084

The exoplanet orbiting this star with a period of 2082 days and quite eccentric orbit at 0.66 was discovered by Sato et al. (2013). Atmospheric parameters were derived by Takeda et al. (2008) using a similar method as described in this paper. The spectra they analyzed however, was not of as high quality as used here. Using the HIDES spectrograph Takeda et al. (2008) reported an average SNR for their sample of 100-300 at a resolving power of 67 000. We used data from ESPaDOnS with a resolving power of 81 000, and with a SNR for this star of 850. With our new parameter we obtain a slightly lower stellar mass for the star at $1.93 M_\odot$ compared to $2.39 M_\odot$ obtained by Takeda et al. (2008), hence the minimum planetary mass is also decreased slightly from $m_{\rm pl} \sin i = 4.5 M_J$ to $m_{\rm pl} \sin i = 3.9 M_J$. We see a decrease in the stellar radius by 28% from $9.12 R_\odot$ to $7.81 R_\odot$. Since there are no observations of the planet transiting, the planetary radius has not been computed.

5.3. HD 233604

HD 233604 b was discovered by Nowak et al. (2013) while the atmospheric parameters of the star were derived by Zieliński et al. (2012) with the same method as described in this paper using the HRS spectrograph with a resolving power of 60 000 with a typical SNR at 200-250. We obtained the spectrum for this star using the FIES spectrograph with a slightly higher resolution at 67 000, and similar but also slightly higher SNR at 320 for this star.

This planet is very close orbit with a semi-major axis of $\sim 15 R_{\rm st}$ ($R_{\rm st}$ is the stellar radius) using the parameters from Nowak et al. (2013). With the updated parameters presented in this paper we see a slight increase in the stellar mass from $1.5 M_\odot$ to $1.9 M_\odot$ and a decrease in stellar radius from $10.5 R_\odot$ to $8.6 R_\odot$. This gives an increase of the semi major axis to $\sim 21 R_{\rm st}$. Note that the correct stellar radius are used to describe the semi-major axis in both cases.

The increase in stellar mass leads to an increase in the minimum planetary mass, from $6.58 M_J$ to $7.79 M_J$.

Nowak et al. (2013) found a high Li abundance at $A(\rm Li) = 1.400 \pm 0.042$ for this star speculating if this star might have engulfed a planet. A more likely explanation is that this star has not yet reached the first dredge-up process (Nowak et al. 2013). We found a much lower value at $A(\mathrm{Li}) = 0.9$ and hence we find the star to not be Li rich. The Li abundance we find is in excellent agreement with Adamów et al. (2014) as we get the same abundance. They also calculate the Li abundance with a non-LTE correction and get $A(\mathrm{Li}) = 1.08$. To understand this star in detail a more detailed abundance study would be needed as well as a precise placement in an HR diagram.

5.4. HD 5583

This exoplanet was discovered by Niedzielski et al. (2016) has an orbital period of 139 days around a K giant. This exoplanet was discovered with the radial velocity technique, hence we do not have a planetary radius. The stellar parameters were derived in a similar manner as presented here (see Niedzielski et al. 2016, and references therein) where our biggest disagreement is in the surface gravity. We derive a 0.34 dex higher $\log g$ giving us a smaller stellar radius (37% smaller). The derived mass is 15% higher which in turn increases the minimum planetary mass from $5.78M_J$ to $8.63M_J$. Even with the increase in mass, it is still within the planetary regime for most inclinations as noted by Niedzielski et al. (2016).

5.5. HD 81688

This exoplanet was discovered by Sato et al. (2008) with the RV method. The host star is a metal-poor K giant. The atmospheric parameters presented in Sato et al. (2008) are from the same method as presented in this paper, and we have quite good agreement. Once again the big disagreement is in the surface gravity where ours is 0.48 dex higher. Even though the stellar parameters, and hence the planetary, does change, the radius and mass we derive are not far from what is presented in the paper by Sato et al. (2008). This is a case where the star was marked as an outlier due to the comparison between the radius and mass derived from Torres et al. (2010).

The new stellar mass is the same as before, $2.1M_\odot$. The stellar radius change from $13.0R_\odot$ to $10.8R_\odot$. Since a transit of this star has not been observed and the stellar mass remains the same, we do not see any change in the planetary parameters.

We note that this system is in an interesting configuration with a very close orbit around an evolved star. This system, among others, have been subject to work on planet engulfment (see e.g. Kunitomo et al. 2011).

5.6. HIP 107773

The planetary companion was presented in Jones et al. (2015) as an exoplanet around an intermediate mass evolved star. The stellar parameters were obtained from the analysis by Jones et al. (2011) using the same method as presented here, however with a different line list which might lead to some disagreements. For this star we derive a higher $\log g$ at 2.83 dex compared to 2.60 dex, and thus we derive a slightly smaller star with $11.6R_\odot$ to $9.2R_\odot$ and $2.4M_\odot$ to $2.1M_\odot$ for radius and mass of the star respectively. The other atmospheric parameters are very similar to those derived by Jones et al. (2011). This leads to a reduced minimum mass of the planetary companion from $m \sin i = 1.98M_J$ to $m \sin i = 1.78M_J$.

5.7. WASP-97

The exoplanet orbiting WASP-97 was discovered by Hellier et al. (2014). The host star parameters were derived in a similar method as described in this paper after co-adding several spectra from the CORALIE spectrograph. They reach a SNR of 100 with a spectral resolution of 50 000. The parameters presented here comes from the UVES spectrograph with a SNR of more than 200.

The parameters does not change much for this planet. The planetary mass is changed from $1.32M_J$ to $1.37M_J$ and the radius from $1.13R_J$ to $1.42R_J$. This does affect the density quite a lot from $1.13\,\mathrm{g/cm^3}$ to $0.59\,\mathrm{g/cm^3}$. This exoplanet is then in the same category as Saturn with a density lower than water, however with a size slightly larger than Jupiter.

5.8. ω Serpentis (ome Ser)

The exoplanet orbiting this star with a period of 277 days and an eccentric orbit at 0.11 was also presented by Sato et al. (2013). The atmospheric parameters were derived in the same way as for HD 120084. We used data from FIES with a resolving power of 67 000, and with a SNR for this star of 1168. With our new parameter we obtain a slightly higher stellar mass for the star at $2.19M_\odot$ compared to $2.17M_\odot$ obtained by Takeda et al. (2008). This change is not significant enough to change the minimum planetary mass at $m_{\mathrm{pl}} \sin i = 1.7m_J$. The stellar radius decrease with more than one solar radius, from $12.3R_\odot$ to $11.1R_\odot$. However, since there are no observations of exoplanet transiting, we can not see the change in the planetary radius.

5.9. omi UMa

omi UMa b was discovered by Sato et al. (2012) using the RV method. The stellar parameters are from Takeda et al. (2008) as discussed above. The spectrum used for this star is from ESPaDOnS with a SNR of more than 500 compared to the 100-300 SNR reached for the large sample presented in Takeda et al. (2008). The luminosity and mass for omi UMa were obtained from theoreitcal evolutionary tracks (see Sato et al. 2012, and references therein). The radius was then estimated using the Stefan-Boltzmann relationship and the measured luminosity and T_{eff}.

The parameters presented here mainly differ in the surface gravity where ours is 0.72 dex higher at $\log g = 3.36$. These leads to a big change in stellar mass and radius from $3.1M_\odot$ to $1.6M_\odot$ and $14.1R_\odot$ to $4.5R_\odot$, respectively. omi UMa b was reported to be the first planet candidate around a star more massive than $3M_\odot$ by Sato et al. (2012). With these updated results, the minimum mass of the planet is now $m \sin i = 2.7M_J$ whereas it was $m \sin i = 4.1M_J$ (Sato et al. 2012). The exoplanet is not reported to transit as seen from Earth, so we do not have a radius for this exoplanet, which would have changes a lot with these new results.

6. Conclusion

With this update we bring the completeness of SWEET-Cat for stars brighter than magnitude 10 (V band) up to 85% (77% for stars brighter than 12). The parameters are available for the public in an easy accessible form at `https://www.astro.up.pt/resources/sweet-cat/` which is continuously updated. The importance of the homogeneous analysis which we keep striving for is shown in Figure 7 where we see quite different derived stellar radius when the atmospheric parameters comes from different methods. As have been discussed in Section 5 this has a direct impact on the planetary parameters. It is of great importance to know the planetary parameters very well, both for individual systems but also for an ensemble. With accurate and precise planetary parameters we will be able to distinguish the different possible composition, let it be gas giant, water worlds, or rocky planets.

Last we also provide an online tool to derive the stellar atmospheric parameters using FASMA. We recommend to only use this tool for spectra and stars where this method is working, i.e. high resolution spectra with a high SNR. The stars can be FGK dwarfs and FGK subgiants/giants. We are working on applying this method in the NIR in order to include M stars in the analysis for the numerous up-comming spectrographs.

Acknowledgements. This work was supported by Fundação para a Ciência e a Tecnologia (FCT) through the research grants UID/FIS/04434/2013 and PTDC/FIS-AST/1526/2014. N.C.S., and S.G.S. acknowledge the support from FCT through Investigador FCT contracts of reference IF/00169/2012, and IF/00028/2014, respectively, and POPH/FSE (EC) by FEDER funding through the program "Programa Operacional de Factores de Competitividade - COMPETE". E.D.M. and B.J.A. acknowledge the support from FCT in form of the fellowship SFRH/BPD/76606/2011 and SFRH/BPD/87776/2012, respectively. This work also benefit from the collaboration of a cooperation project FCT/CAPES - 2014/2015 (FCT Proc 4.4.1.00 CAPES). AM received funding from the European Union Seventh Framework Programme (FP7/2007-2013) under grant agreement number 313014 (ETAEARTH). This research has made use of the SIMBAD database operated at CDS, Strasbourg (France).

References

Adamów, M., Niedzielski, A., Villaver, E., Wolszczan, A., & Nowak, G. 2014, A&A, 569, A55

Adibekyan, V. Z., Benamati, L., Santos, N. C., et al. 2015, MNRAS, 450, 1900

Adibekyan, V. Z., Sousa, S. G., Santos, N. C., et al. 2012, A&A, 545, A32

Anders, E. & Grevesse, N. 1989, Geochim. Cosmochim. Acta, 53, 197

Andreasen, D. T., Sousa, S. G., Delgado Mena, E., et al. 2016, A&A, 585, A143

Dekker, H., D'Odorico, S., Kaufer, A., Delabre, B., & Kotzlowski, H. 2000, in Proc. SPIE, Vol. 4008, Optical and IR Telescope Instrumentation and Detectors, ed. M. Iye & A. F. Moorwood, 534–545

Donati, J.-F. 2003, in Astronomical Society of the Pacific Conference Series, Vol. 307, Solar Polarization, ed. J. Trujillo-Bueno & J. Sanchez Almeida, 41

Frandsen, S. & Lindberg, B. 1999, in Astrophysics with the NOT, ed. H. Karttunen & V. Piirola, 71

Gonzalez, G. & Laws, C. 2000, AJ, 119, 390

Gray, D. F. 2005, The Observation and Analysis of Stellar Photospheres, 3rd ed.

Gustafsson, B., Edvardsson, B., Eriksson, K., et al. 2008, A&A, 486, 951

Hartman, J. D., Bakos, G. Á., Torres, G., et al. 2014, AJ, 147, 128

Hellier, C., Anderson, D. R., Cameron, A. C., et al. 2014, MNRAS, 440, 1982

Jones, M. I., Jenkins, J. S., Rojo, P., & Melo, C. H. F. 2011, A&A, 536, A71

Jones, M. I., Jenkins, J. S., Rojo, P., Olivares, F., & Melo, C. H. F. 2015, A&A, 580, A14

Kaufer, A., Stahl, O., Tubbesing, S., et al. 1999, The Messenger, 95, 8

Kunitomo, M., Ikoma, M., Sato, B., Katsuta, Y., & Ida, S. 2011, ApJ, 737, 66

Kurucz, R. 1993, ATLAS9 Stellar Atmosphere Programs and 2 km/s grid. Kurucz CD-ROM No. 13. Cambridge, Mass.: Smithsonian Astrophysical Observatory, 1993., 13

Mayor, M., Pepe, F., Queloz, D., et al. 2003, The Messenger, 114, 20

Mészáros, S., Allende Prieto, C., Edvardsson, B., et al. 2012, AJ, 144, 120

Mortier, A., Santos, N. C., Sousa, S., et al. 2013, A&A, 551, A112

Mortier, A., Sousa, S. G., Adibekyan, V. Z., Brandão, I. M., & Santos, N. C. 2014, A&A, 572, A95

Neves, V., Santos, N. C., Sousa, S. G., Correia, A. C. M., & Israelian, G. 2009, A&A, 497, 563

Niedzielski, A., Villaver, E., Nowak, G., et al. 2016, A&A, 588, A62

Nowak, G., Niedzielski, A., Wolszczan, A., Adamów, M., & Maciejewski, G. 2013, ApJ, 770, 53

Pourbaix, D., Tokovinin, A. A., Batten, A. H., et al. 2004, A&A, 424, 727

Santos, N. C., Israelian, G., Mayor, M., Rebolo, R., & Udry, S. 2003, A&A, 398, 363

Santos, N. C., Sousa, S. G., Mortier, A., et al. 2013, A&A, 556, A150

Sato, B., Izumiura, H., Toyota, E., et al. 2008, PASJ, 60, 539

Sato, B., Omiya, M., Harakawa, H., et al. 2012, PASJ, 64 [e-prints[arXiv]1207.3141]

Sato, B., Omiya, M., Harakawa, H., et al. 2013, PASJ, 65 [e-prints[arXiv]1304.4328]

Sneden, C. A. 1973, PhD thesis, THE UNIVERSITY OF TEXAS AT AUSTIN.

Sousa, S. G., Santos, N. C., Adibekyan, V., Delgado-Mena, E., & Israelian, G. 2015, A&A, 577, A67

Sousa, S. G., Santos, N. C., & Israelian, G. 2012, A&A, 544, A122

Sousa, S. G., Santos, N. C., Israelian, G., Mayor, M., & Udry, S. 2011, A&A, 533, A141

Sousa, S. G., Santos, N. C., Mayor, M., et al. 2008, A&A, 487, 373

Takeda, Y., Sato, B., & Murata, D. 2008, PASJ, 60, 781

Torres, G., Andersen, J., & Giménez, A. 2010, A&A Rev., 18, 67

Torres, G., Fischer, D. A., Sozzetti, A., et al. 2012, ApJ, 757, 161

Tsantaki, M., Sousa, S. G., Adibekyan, V. Z., et al. 2013, A&A, 555, A150

Zieliński, P., Niedzielski, A., Wolszczan, A., Adamów, M., & Nowak, G. 2012, A&A, 547, A91

Table .1. The derived parameters for the 66 stars in our sample. The SNR is measured by ARES.

Star	$T_{\rm eff}$ (K)	$\log g$ (dex)	[Fe/H] (dex)	$\xi_{\rm micro}$ (km/s)	$\xi_{\rm micro}$ fixed?	Instrument	SNR
11 Com	4903 ± 34	2.55 ± 0.13^{a}	−0.23 ± 0.03	1.56 ± 0.04	no	FIES	966
14 And	4808 ± 39	2.61 ± 0.10^{a}	−0.22 ± 0.03	1.60 ± 0.04	no	FIES	724
42 Dra	4528 ± 57	2.27 ± 0.11^{a}	−0.30 ± 0.03	1.53 ± 0.05	no	FIES	645
BD -11 4672	4553 ± 75	4.87 ± 0.51	−0.30 ± 0.02	0.14 ± 0.07	yes	FIES	487
BD +49 828	5015 ± 36	2.87 ± 0.09^{a}	−0.01 ± 0.03	1.48 ± 0.04	no	FIES	567
GJ 785	5087 ± 48	4.42 ± 0.10	−0.01 ± 0.03	0.69 ± 0.10	no	HARPS	801
HATS-1	5969 ± 46	4.39 ± 0.06	−0.04 ± 0.04	1.06 ± 0.08	no	UVES	155
HATS-5	5383 ± 91	4.41 ± 0.22	0.08 ± 0.06	0.91 ± 0.14	no	UVES	158
HAT-P-12	4642 ± 106	4.53 ± 0.27	−0.26 ± 0.06	0.28 ± 0.63	no	FIES	185
HAT-P-24	6470 ± 181	4.33 ± 0.27	−0.41 ± 0.10	1.40 ± 0.03	yes	UVES	158
HAT-P-39	6745 ± 236	4.39 ± 0.47	−0.21 ± 0.12	1.53 ± 0.04	yes	UVES	127
HAT-P-42	5903 ± 66	4.29 ± 0.10^{a}	0.34 ± 0.05	1.19 ± 0.08	no	UVES	130
HAT-P-46	6421 ± 121	4.53 ± 0.14^{a}	0.16 ± 0.09	1.67 ± 0.18	no	UVES	208
HD 102272	4883 ± 34	2.69 ± 0.07^{a}	−0.29 ± 0.03	1.54 ± 0.04	no	FIES	1011
HD 104985	4786 ± 58	2.66 ± 0.09^{a}	−0.28 ± 0.04	1.65 ± 0.05	no	FIES	1010
HD 114762	5879 ± 39	4.23 ± 0.04^{a}	−0.66 ± 0.03	1.16 ± 0.07	no	FIES	1671
HD 120084	4969 ± 40	2.94 ± 0.14^{a}	0.12 ± 0.03	1.41 ± 0.04	no	ESPaDOnS	852
HD 152581	5181 ± 27	3.37 ± 0.06^{a}	−0.23 ± 0.02	1.15 ± 0.03	no	FIES	796
HD 155358	5906 ± 33	4.24 ± 0.03^{a}	−0.61 ± 0.02	1.30 ± 0.05	no	FIES	424
HD 171028	5699 ± 36	3.83 ± 0.03^{a}	−0.40 ± 0.02	1.21 ± 0.04	no	FIES	460
HD 192263	4946 ± 46	4.61 ± 0.14	−0.05 ± 0.02	0.66 ± 0.12	no	HARPS	415
HD 192699	5208 ± 27	3.56 ± 0.10^{a}	−0.12 ± 0.02	1.19 ± 0.03	no	FIES	776
HD 197037	6233 ± 45	4.22 ± 0.04	−0.12 ± 0.03	1.22 ± 0.06	no	FIES	1074
HD 200964	5083 ± 24	3.32 ± 0.07^{a}	−0.16 ± 0.02	1.18 ± 0.03	no	FIES	1081
HD 219134	4767 ± 70	4.57 ± 0.17	0.00 ± 0.04	0.59 ± 0.24	no	ESPaDOnS	725
HD 220074	4748 ± 233	3.67 ± 0.33^{a}	−0.06 ± 0.09	2.82 ± 0.37	no	FIES	419
HD 220842	5999 ± 39	4.30 ± 0.06^{a}	−0.08 ± 0.03	1.21 ± 0.05	no	FIES	459
HD 233604	4954 ± 46	2.86 ± 0.11^{a}	−0.14 ± 0.04	1.61 ± 0.05	no	FIES	314
HD 283668	4841 ± 73	4.51 ± 0.18	−0.74 ± 0.04	0.16 ± 0.61	no	FIES	592
HD 285507	4620 ± 126	4.72 ± 0.61	0.04 ± 0.06	0.74 ± 0.43	no	UVES	239
HD 37124	5460 ± 35	4.24 ± 0.04	−0.42 ± 0.03	0.61 ± 0.07	no	FIES	988
HD 5583	4986 ± 35	2.87 ± 0.09^{a}	−0.35 ± 0.03	1.62 ± 0.04	no	FIES	933
HD 70573	5889 ± 186	4.32 ± 0.27^{a}	−0.42 ± 0.13	1.14 ± 0.01	yes	FIES	487
HD 81688	4903 ± 21	2.70 ± 0.05^{a}	−0.21 ± 0.02	1.54 ± 0.02	no	[b]	1350, 860
HD 82886	5123 ± 18	3.30 ± 0.04^{a}	−0.25 ± 0.01	1.16 ± 0.02	no	[c]	1198,1294
HD 96063	5232 ± 36	3.61 ± 0.06^{a}	−0.12 ± 0.03	1.23 ± 0.04	no	FIES	644
HD 97658	5219 ± 54	4.60 ± 0.10	−0.28 ± 0.04	0.78 ± 0.11	no	FIES	1123
HD 87883	4917 ± 68	4.53 ± 0.19	0.02 ± 0.03	0.46 ± 0.21	no	ESPaDOnS	753
HIP 107773	4957 ± 49	2.83 ± 0.09^{a}	0.04 ± 0.04	1.49 ± 0.05	no	UVES	218
HIP 11915	5770 ± 14	4.33 ± 0.03	−0.06 ± 0.01	0.95 ± 0.02	no	HARPS	709
HIP 116454	5038 ± 82	4.53 ± 0.18	−0.12 ± 0.04	0.74 ± 0.15	no	FIES	309
HR 228	5042 ± 42	3.30 ± 0.09^{a}	0.07 ± 0.03	1.14 ± 0.04	no	UVES	400
KELT-6	6246 ± 88	4.22 ± 0.09^{a}	−0.22 ± 0.06	1.66 ± 0.13	no	FIES	374
Kepler-37	5378 ± 53	4.47 ± 0.12	−0.23 ± 0.04	0.58 ± 0.13	no	FIES	205
Kepler-444	5111 ± 43	4.50 ± 0.13	−0.51 ± 0.03	0.37 ± 0.15	no	FIES	675
ksi Aql	4834 ± 42	2.65 ± 0.10^{a}	−0.14 ± 0.03	1.53 ± 0.04	no	FIES	919
mu Leo	4605 ± 94	2.61 ± 0.26^{a}	0.25 ± 0.06	1.64 ± 0.11	no	ESPaDOnS	354
ome Ser	4928 ± 35	2.69 ± 0.06^{a}	−0.11 ± 0.03	1.55 ± 0.04	no	FIES	1168
omi CrB	4882 ± 40	2.64 ± 0.10^{a}	−0.17 ± 0.03	1.55 ± 0.04	no	FIES	932
omi UMa	5499 ± 52	3.36 ± 0.07^{a}	−0.01 ± 0.05	1.98 ± 0.06	no	ESPaDOnS	527
Qatar-2	4637 ± 316	4.53 ± 0.62	0.09 ± 0.17	0.63 ± 0.83	no	UVES	97
SAND364	4457 ± 104	2.26 ± 0.20^{a}	−0.04 ± 0.06	1.60 ± 0.11	no	UVES	220
TYC+1422-614-1	4908 ± 41	2.90 ± 0.12^{a}	−0.07 ± 0.03	1.57 ± 0.05	no	FIES	506
WASP-37	5917 ± 72	4.25 ± 0.15	−0.23 ± 0.05	0.59 ± 0.13	no	FIES	232
WASP-44	5612 ± 80	4.39 ± 0.30	0.17 ± 0.06	1.32 ± 0.13	no	UVES	125
WASP-52	5197 ± 83	4.55 ± 0.30	0.15 ± 0.05	1.16 ± 0.14	no	UVES	125
WASP-58	6039 ± 55	4.23 ± 0.10	−0.09 ± 0.04	1.12 ± 0.08	no	FIES	310

Table .1. continued.

WASP-61	6265 ± 168	4.21 ± 0.21[a]	−0.38 ± 0.11	1.44 ± 0.02	yes	UVES	163
WASP-72	6570 ± 85	4.25 ± 0.13	0.15 ± 0.06	2.30 ± 0.15	no	UVES	174
WASP-75	6203 ± 46	4.42 ± 0.22[a]	0.24 ± 0.03	1.45 ± 0.06	no	UVES	189
WASP-76	6347 ± 52	4.29 ± 0.08[a]	0.36 ± 0.04	1.73 ± 0.06	no	UVES	165
WASP-82	6563 ± 55	4.29 ± 0.10[a]	0.18 ± 0.04	1.93 ± 0.08	no	UVES	239
WASP-88	6450 ± 61	4.24 ± 0.06[a]	0.03 ± 0.04	1.79 ± 0.09	no	UVES	174
WASP-95	5799 ± 31	4.29 ± 0.05[a]	0.22 ± 0.03	1.18 ± 0.04	no	UVES	247
WASP-97	5723 ± 52	4.24 ± 0.07	0.31 ± 0.04	1.03 ± 0.08	no	UVES	219
WASP-99	6324 ± 89	4.34 ± 0.12	0.27 ± 0.06	1.83 ± 0.12	no	UVES	249

Notes. [a] Spectroscopic $\log g$. [b] Weighted average of ESPaDoNS and FIES results. The parameters are (FIES in parantheses): $T_{\rm eff}$ = 4870(4934) ± 30(29), $\log g$ = 2.50(2.73) ± 0.14(0.05), [Fe/H] = −0.26(−0.19) ± 0.03(0.02), and $\xi_{\rm micro}$ = 1.50(1.59) ± 0.03(0.03). [c] Weighted average of ESPaDoNS and FIES results. The parameters are (FIES in parantheses): $T_{\rm eff}$ = 15124(5121) ± 22(29), $\log g$ = 3.30(3.31) ± 0.05(0.07),